LIST OF TABLES

LIST OF ABBREVIATIONS

NAHRIM	National Hydraulic Research Institute of Malaysia
AOP	Advance oxidation process
PET	Polyethelene terephthalate
SEM	Scanning electron microscope
TEM	Transmission electron microscope
EDX	Electron diffraction X-rays
XRD	X-rays diffraction
RhB	Rhodamine B
UV-Vis	UV Vis spectrometer
SAED	Selected area electron diffraction
WQI	Water Quality Index
NWQS	National Water Quality Standards
DO	Dissolved oxygen
BOD	Biochemical oxygen demand
COD	Chemical oxygen demand
SS	Suspended solids
PCT	Physic-chemical treatment
NDP	Net driving pressure
NHE	Normal Hydrogen Electrode
PL	Photoluminescence
TA	Terephthalic acid
MB	Methylene blue

DALY	Deaths and disability adjusted life year
TCO	Transparent and conducting oxide
FCC	Face-centered cubic
D	Proton diffusion coefficient
TEP	Thermoelectric power
XPS	X-ray photoelectron spectroscopy
FTIR	Fourier transform infrared spectroscopy

LIST OF SYMBOLS

P_{osm}	*Osmosis pressure*
T	Temperature
m_i	Molar concentration
Q_w	Rate of water flow
P	Pressure
E_c	Conduction band
E_v	Valence Band
E_g	Energy bandgap
E_{AVS}	Absolute vacuum scale of semiconductor

PUBLICATIONS

Academic Journals (International)

1. **Y.L. Chan**, S.Y. Pung and S. Sreekantan, "Degradation of Organic Dye using ZnO nanorods based Continuous Flow Water Purifier, J. Sol-Gel Sci. Tech. (2013) 399-405. (ISI cited, impact factor: 1.632).
2. **Y.L. Chan**, S.Y. Pung, N.S. Hussain, S. Sreekantan and F.Y. Yeoh, "Photocatalytic Degradation of Rhodamine B using MnO_2 and ZnO Nanoparticles" Mater. Sci. Forum 756 (2013) 167-714. (ISI cited)

Conference Proceeding (International)

1. **Y.L. Chan**, S.Y. Pung, S. Sreekantan and F.Y. Yeoh, "ZnO-MnO_2 Core-Shell Nanocomposites as a Promising Visible-Light Driven Photocatalyst for Pollutants Removal" 223rd ECS Meeting, Toronto, Ontario, Canada (May 12-16, 2013).
2. **Y.L. Chan**, S.Y. Pung and S. Sreekantan, "Comparative Study Of ZnO And V_2O_5 Nanoparticles As Heterogeneous Photocatalysts In Degrading Organic Pollutants", Proceeding of the 5th Regional Conference on Materials Engineering and the 5th Regional Conference on Natural Resources and Materials 2013 (RCM5 & RCNRM5) (21-23 Jan 2013).
3. **Y.L. Chan**, S.Y. Pung, F.Y. Yeo, S. Sreekantan and N.S. Hussain, "Degradation of Rhodamine B using Semiconductor Nanoparticles with Different Bandgap Energy as photocatalyst", The 3rd ISESCO International Workshop and Conference on Nanotechnology (IWCN 2012), Kuala Lumpur, Malaysia (5-7 Dec 2012).

SINTESIS DAN PENCIRIAN BAGI FOTOPEMANGKIN NANOSTRUKTUR ZnO, V_2O_5 DAN MnO_2 DI ATAS GENTIAN POLIETILENA TERAFTALAT (PET) UNTUK MENGDEGRADASI PERWARNA RhB.

ABSTRAK

Pencemaran sistem pengairan semakin meruncing, terutamanya disebabkan oleh industri textile dan industri pertanian. Hal ini menggugat tahap kesihatan masyarakat seluruh dunia. Proses pengoksidaan termaju merupakan proses yang sedang membangun di dalam penyelidikan, bertujuan untuk dalam mengdegradasi bahan pencemar organik. Kaedah ini menggunakan tindak balas antara permukaan semikonduktor dengan cahaya ultraungu atau cahaya nyata. Bagi menggunakan cahaya matahari dengan sepenuhnya untuk mengdegradasikan bahan pencemar organik, aktiviti fotokatalisis semikonduktor yang mempunyai nilai jurang besar (ZnO, $E_g = 3.37$ eV) dan nilai jurang kecil (MnO_2, $E_g = 1.00$ hingga 1.80 eV dan V_2O_5, $E_g = 2.50$ eV) di bawah sinaran ultraungu dan cahaya nyata telah dikaji. Nanorod ZnO dan nanorod V_2O_5 telah disediakan melalui kaedah sol-gel, sebaliknya nano partikal MnO_2 polimorf disintesis melalui kaedah hidrotermal dengan penyesuaian nisbah antara $KMnO_4$ dan $MnSO_4$. Kaedah kinetik terbit pertama digunakan untuk proses fotodegradasi larutan RhB oleh semikonduktor nano partikal tersebut. Di bawah sinaran ultraungu, ZnO memiliki kecekapan fotodegradasi yang baik (0.034 min^{-1}). V_2O_5 (0.0149 min^{-1}) dan MnO_2 (0.0221 min^{-1}) mempunyai kadar fotodegradasi yang lebih bagus dalam proses penyikiran pewarna RhB di bawah cahaya nyata. Modelfotodegradasi larutan RhB yang telah diperhalusi dengan fotopemangkin semikonduktor tersebut telah dicadangkan. Dua proses, iaitu N-deethylsasi dan cycloreversi berlaku secara serentak dalam proses fotodegradasi larutan RhB. Bedasarkan keputusan ujikaji proses cycloreversi menjadi dominan apabila nanopartikal ZnO dan V_2O_5 digunakan sebagai fotopemangkin yang menyebabkan larutan RhB mengalami mineralsasi yang lengkap. Sebaliknya, N-deethylsasi menjadi dominan apabila nanopartikal MnO_2 digunakan sebagai fotopemangkin dan larutan RhB menunjukkan peringkat peralihan yang jelas (menjadi warna kehijauan) sebelum ia dinyahwarnakan secara lengkap. Seterusnya, bahan nano semikonduktor ini telah ditumbuhkan di atas gentian PET yang fleksibel untuk meminimumkan bahan tersebut daripada dialirkan keluar oleh air dan untuk mengelakkan campuran bahan itu ke dalam sistem pengairan semasa proses rawatan fotokatalitik. Hal ini mungkin akan menyebabkan pecemaran sekunder di dalam sistem pengairan dan lama-kelamaan merosotkan kecekapan proses fotodegradasi tersebut. Nanorod ZnO dengan nisbah aspek (17.1 ± 3.99) telah ditumbuhkan di atas gentian PET. Di bawah sinaran ultraungu, kecekapan fotodegradasi nanorod ZnO pada gentian PET untuk mengdegradasikan peredaran larutan RhB dengan ialah 0.022 min^{-1}. Di bawah sinaran nyata, β-MnO_2 nanorod pada gentian PET adalah terbaik berbanding V_2O_5 nanokepingan pada gentian PET dengan kadar pemalar 0.2047 min^{-1}. Ia juga berbaloi menyatakan bahawa gentian PET masih dipenuhi oleh semikonductor selepas beberapa jam di bawah larutan RhB kerana mereka masih melekat pada gentian PET. Oleh itu, ZnO nanorod and β-MnO_2 nanorod yang ditumbuhkan pada gentian PET dapat digunakan sebagai fotopemangkan untuk mendegradasi sebatian organik di dalam aplikasi penulenan air.

SYNTHESIS AND CHARACTERIZATION OF ZnO, V_2O_5 AND MnO_2 NANOSTRUCTURES PHOTOCATALYSTS ON POLYETYLENE TEREPHTHALATE (PET) FIBER FOR DEGRADATION OF RhB DYE

ABSTRACT

Increasing pollution into the water system particularly from textile industries and agriculture has become a source of health concern across the globe. Advanced oxidation process is a rapid developing research field for the application in degradation of organic pollutants. This approach utilizes the reaction on the semiconductor's surface in the presence of UV or visible light irradiation. In order to utilize sunlight effectively for organic pollutants removal, the photocatalytic activities of wide bandgap semiconductor (ZnO, E_g =3.37 eV) and narrow bandgap semiconductors (MnO_2, E_g = 1.00 to 1.80 eV and V_2O_5, E_g = 2.50 eV) under UV light or visible light irradiation were studied. The ZnO nanorods and V_2O_5 nanorods were prepared by sol-gel method whereas different polymorphs of MnO_2 nanoparticles were synthesized using hydrothermal method by adjusting the ratio of $KMnO_4$ and $MnSO_4$. The photodegradation of RhB solution by these semiconductor nanoparticles followed first order kinetic. Under UV irradiation, ZnO has good photodegradation efficiency (0.034 min^{-1}). On the other hand, V_2O_5 nanorods and β-MnO_2 nanoparticles degraded RhB dye under visible light with rate constant of 0.015 min^{-1} and 0.022 min^{-1} respectively. A refined photodegradation model of RhB solution by these semiconductor photocatalysts is proposed. Two processes, i.e. N-deethylation and cycloreversion happen simultaneously during the photodegradation of RhB solution. Based on the results, cycloreversion was dominant when ZnO and V_2O_5 nanoparticles were used

as photocatalysts, causing complete mineralization of RhB solution. In contrary, N-deethylation was dominant when MnO_2 nanoparticles were used as photocatalysts as the RhB solution showed a clear transition stage (turned to greenish color) before decolorized completely. Next, these semiconductors nanomaterials were grown on flexible PET fiber to minimize them from being drained away by water and are charged into water system during the photocatalytic treatment. This could result of forming secondary pollution in the water system and deterioration of photodegradation efficiency over time. ZnO nanorods with high aspect ratio (17.1 ± 3.99) were grown on PET fiber. Under UV irradiation, photodegradation efficiencies of ZnO nanorods on PET fiber to degrade circulated RhB solution was 0.022 min^{-1}. Under visible light irradiation, β-MnO_2 nanotubes on PET fiber is a better photocatalyst as compared to V_2O_5 nanoflakes on PET fiber as it has a larger rate constant, i.e. 0.2047 min^{-1}. It is worth mentioning that the PET fibers were still covered by oxide semiconductors after several hour circulation of RhB solution, indicating that they adhered well on the PET fiber. Thus, both ZnO nanorods and β-MnO_2 nanotubes that grown on PET fiber could be used as photocatalysts for water purification application to degrade organic compounds.

1.0 INTRODUCTION

1.1 Research Background

Water pollution is a global issue especially in developing country such as Malaysia. It refers to contamination of microorganism, organic and inorganic compounds directly or indirectly discharge into the water body. Water pollution is monitored based on water quality index (WQI). The major parameters which are monitored under WQI are biochemical oxygen demand (BOD), ammonia nitrogen (NH_3-N) and suspended solids (SS). According to the statistical data released by Department of Environmental Malaysia (DOE), the percentage of polluted rivers has been increased from 43.1 % (year 2005) to 48.6 % (year 2010). In 2011, the percentage of polluted rivers has been reduced to 40.7 %, but many rivers still show unhealthy water pollution level. Out of 464 rivers monitored in Malaysia at 2011, 275 rivers (59.3 %) were found to be clean, 150 rivers (32.3 %) were slightly polluted and 39 rivers (8.4 %) were polluted. The pollution sources are claimed attributing to the population growth, untreated sewage, urbanization, industrialization and expansion of agriculture (Sharifuddin, 2011).

Waste water treatment is designed to remove contaminants from water body and to improve the quality of water. For instances, municipal wastewater treatment (Liu and Lipták, 2000) and reverse osmosis (Mark, 2007) are used to purify water. Although the quality of water has been improved, these water treatments could cause several side effects to the environment and human. For examples, water molecules become more acidic and larger than the natural water molecules after reverse osmosis process. When the water molecules become acidic, most of the minerals such as calcium, magnesium and potassium are stripped off from our body in order to neutralize the water. On the other hand, the municipal water treatment is poor in removing organic pollutants from waste water and killing bacteria. This approach requires a long period of time to remove the pollutants.

Advance oxidation process (AOP) is one of the approaches for organic pollutants removal. It is also known as photocatalytic activity which utilizes the reaction on the semiconductor's surface in the presence of UV or visible light irradiation to degrade organic pollutants. AOP is a simple and low cost process. It produces less harmful by-products to the environment after the process. The charge carriers (electrons and holes) are generated when the light source has energy which is larger than the bandgap of semiconductor. These charge carriers produce free radicals that are required to degrade the organic compounds.

Although most of the semiconductors can undergo photocatalytic activity, oxide semiconductors such as zinc oxide (ZnO) (Hong *et al.*, 2009) and titanium oxide (TiO_2) (Ishibashi *et al.*, 2000) are more preferable because of their wide bandgap which is sensitive to UV light irradiation. Recently, visible light driven semiconductors for photocatalytic activity have been greatly studied because our solar spectrum consists of 44 % of visible light irradiation and approximately 3 % of UV irradiation. Generally, these visible light driven semiconductors can be produced by 3 methods i.e.: (i) doped wide bandgap semiconductor such as CdO doped ZnO (Yousef *et al.*, 2012), Cu doped ZnO (Mohan *et al.*, 2012) and C doped ZnO (Liu *et al.*, 2011), (ii) core-shell nanocomposites (CSNs) such as ZnO-CdS CSNs (Wang *et al.*, 2010) and MnO-ZnO CSNs (Zhang *et al.*, 2012a) and (iii) narrow bandgap oxide semiconductors such as MnO_2 (Cao and Suib, 1994) and V_2O_5 (Wang *et al.*, 2008c).

These oxide semiconductors can be synthesized via solution route such as sol gel approach (Lakshmi *et al.*, 1997), hydrothermal (Laudise and Ballman, 1960, Chandrappa *et al.*, 2003, Cao *et al.*, 2010) and electrodeposition. (Kishwar *et al.*, 2011). Solution route is preferred because of its low synthesis temperature, good morphology control, low cost process and possibility of mass production.

1.2 Problem Statement

Degradation of organic pollutants using wide bandgap semiconductor nanoparticles as photocatalysts have been widely studied in the past few years. However there are a few major issues using these semiconductor nanoparticles for water purification application.

a) Low photodegradation efficiency under visible light

Wide bandgap semiconductors such as TiO_2, CdS, and ZnO are only sensitive to UV light. Although the efficiency of degradation of organic dye in lab scale (using UV lamp) is promising, it is not good enough when it is used under sunlight as the solar spectrum only composes of ~ 3 % of UV light. It is about 44 % energy of visible light is not being used for photocatalytic activity.

b) Separation process of nanoparticles from slurry is complicated and costly

It is necessary to remove the semiconductor nanoparticles from slurry after the degradation process. This is normally accomplished by centrifugation and is time consuming. The need for such additional processing step for removal of material from the slurry can be avoided by depositing thin film or nanowire arrays on a rigid substrate such as Si wafers or wire mesh. However, using rigid substrates reduce the flexibility of immersing the photocatalysts into the reservoir module of polluted water.

c) Low yield after long degradation process

The semiconductor nanoparticles tend to drain away by water during the wastewater treatment. Thus, the number of semiconductor nanoparticles during water treatment process is decreased over time. Eventually, the photodegradation efficiency of organic pollutants via photocatalytic activity is deteriorated.

These issues can be rectified by growing semiconductor nanomaterials on flexible fiber such as polyethylene terephthalate (PET). Besides, PET is a recyclable material. The semiconductor nanomaterial grown on fiber shall be able to last longer without draining away during water purification process. Besides, semiconductor nanomaterials such as MnO_2 and V_2O_5 that sensitive to visible light shall be developed to improve the photodegradation efficiency of organic pollutants.

1.3 Research Objectives

The objectives of this research work study are as follows:

a) To synthesize and characterize ZnO nanoparticles (UV light response), V_2O_5 and MnO_2 nanoparticles (visible light response) using solution route (sol gel method and hydrothermal).

b) To synthesize and characterize these nanomaterials onto PET fiber using sol gel method.

c) To study the photocatalytic activity of these nanomaterials in degrading organic dye (Rhodamine B, RhB).

1.4 Project Overview

This project is divided into two phases in order to achieve the objectives.

Phase 1: Synthesis of UV light driven photocatalysts and visible light driven photocatalysts nanoparticles.

ZnO (UV light driven photocatalysts), V_2O_5 and MnO_2 (visible light driven photocatalysts) nanoparticles were synthesized using solution route such as sol-gel process and hydrothermal. The structural and optical properties of as-synthesized ZnO nanoparticles were characterized by SEM/EDS, XRD, PL and UV-Vis spectroscopy.

The effectiveness of nanoparticles to degrade organic dye (RhB) under UV (254 nm) or visible light irradiation (555 nm) was studied. RhB was chosen because it is a common xanthene dye used in textile which caused environment pollution. The photodegradation efficiency of (i) ZnO nanoparticles (ii) V_2O_5 nanoparticles and (iii) MnO_2 nanoparticles were evaluated. This was done by measuring the maximum absorption wavelength of RhB solution as a function of UV or visible light irradiation duration using UV-Vis spectrometer (Cary 50) at room temperature.

Phase 2: Synthesis of UV light driven photocatalysts and visible light driven photocatalysts nanostructure on PET fiber.

ZnO (UV light driven photocatalysts), V_2O_5 and MnO_2 (visible light driven photocatalysts) nanoparticles were grown on PET fiver via solution route. The structural and optical properties of as-synthesized nanomaterials are characterized by SEM/EDS, XRD, PL and UV-Vis spectroscopy.

The effectiveness of these nanomaterials to degrade RhB under UV or visible light irradiation was studied. The photocatalytic activities of (i) semiconductor nanoparticles which grown on PET fiber (RhB solution under stagnant condition) and (ii) semiconductor nanoparticles which grown on PET fiber (RhB solution under circulation condition) were evaluated. This was done by measuring the maximum absorption wavelength of RhB solution as a function of UV or visible light irradiation duration using UV-Vis spectrometer (Cary 50) at room temperature.

This project overview is summarized in Figure 1.1.

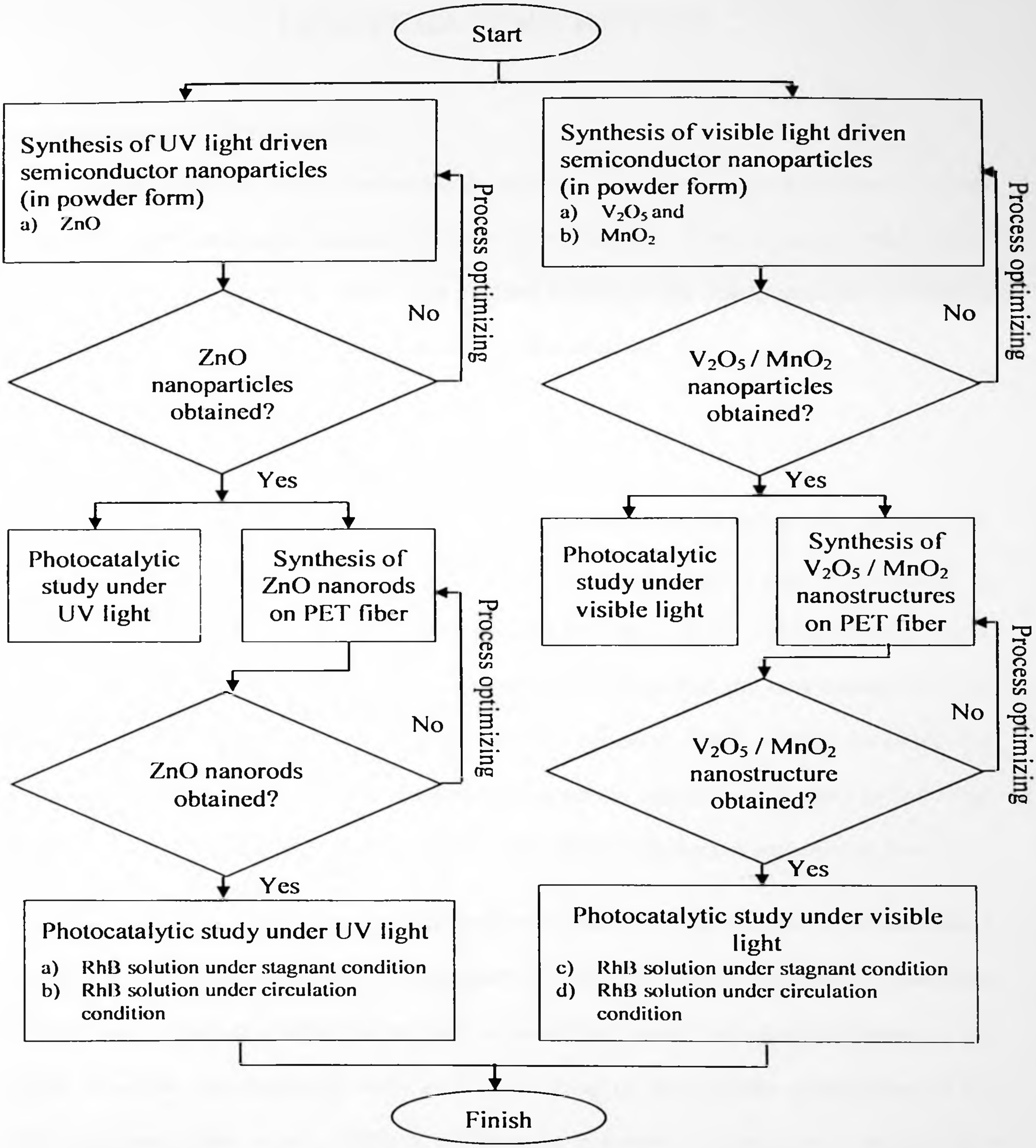

Figure 1.1: Flow chart of project.

2.0 LITERATURE REVIEW

2.1 Semiconductor Photocatalysts

Oxide semiconductor nanomaterials are very effective in photocatalytic activity under UV light irradiation because of their wide bandgap. Thus, structural and optical properties of oxide semiconductors such as zinc oxide (ZnO), manganese oxide (MnO_2) and vanadium oxide (V_2O_5) will be discussed in this section.

2.1.1 Zinc Oxide (ZnO) Nanoparticles

ZnO has been investigated since 1912. The work done in this period of time was reviewed by Miller (Miller, 1950) and Brown (Brown, 1957). ZnO is conventional used as additive in the rubber of car tyres. It has a positive influence on the vulcanization process. It also considerably improves the heat conductivity by dissipating the heat attributed to the deformation when the tyre contacts the road. In concrete, ZnO powder pro-long the processing time and improves the resistance of concrete against water. ZnO powder can also be used as UV-blocker in sun lotions or as an additive to human and animal food.

The present development of ZnO research started in the middle of 1990s. Many research works have been done on the growth of epitaxial layers, nanowires or quantum dots for various potential applications such as transparent electronic circuits (Hwang *et al.*, 2010), blue/UV optoelectronics such as light-emitting or laser diodes (Mandalapu *et al.*, 2008, Subrahmanyam *et al.*, 2010), a radiation hard material for electronic devices in a hostile environment (Grätzel, 2005), a ferromagnetic material (doped with Mn, Fe, and V) for spintronics applications (Imnamdar *et al.*, 2011, Pooja *et al.*, 2012), and a highly conducting and transparent oxide film (TCO) (Mousavi *et al.*, 2011).

2.1.1.1 Structural and Chemical Bonding of ZnO Nanoparticles

ZnO which also known as zincate is a II-IV compound semiconductor. It presents in three different polymorphs: cubic rocksalt (Rochelle salt), zinc blend and hexagonal wurtzite as illustrated in Figure 2.1. For zinc blend and hexagonal wurtzite, the polymorphs compose of covalent chemical binding with sp^3 hybridisation as shown in Figure 2.2. The anion is surrounded by 4 cations at the corner. Hexagonal wurtzite crystal structure is the most stable in ambient condition among them. The lattice parameters a and b of wurtzite structure have equal length (0.3249 nm) which lie in the x-y axis. The c lattice parameter (0.5208 nm) is parallel to z-axis (Hadis and Umit, 2009). ZnO hexagonal wurtzite structure can be converted to rocksalt structure at relatively high pressure and vice versa (Thareja and Mohanta, 2010). The rocksalt crystal structure consists of two face-centered cubic (FCC) sublattices, shifted along one half of the diagonal of the primitive unit cell against each other. It's lattice is six fold coordinated (Bundesmann *et al.*, 2008).

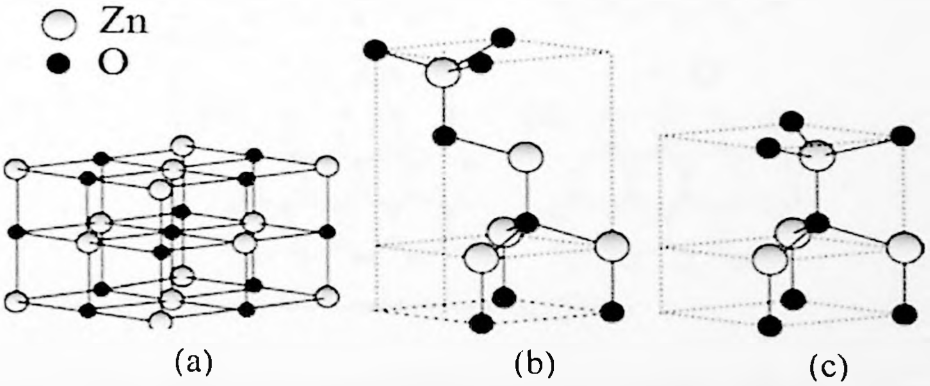

Figure 2.1: ZnO polymorphs: (a) cubic rocksalt, (b) zinc blend and (c) wurtzite (Hadis and Umit, 2009).

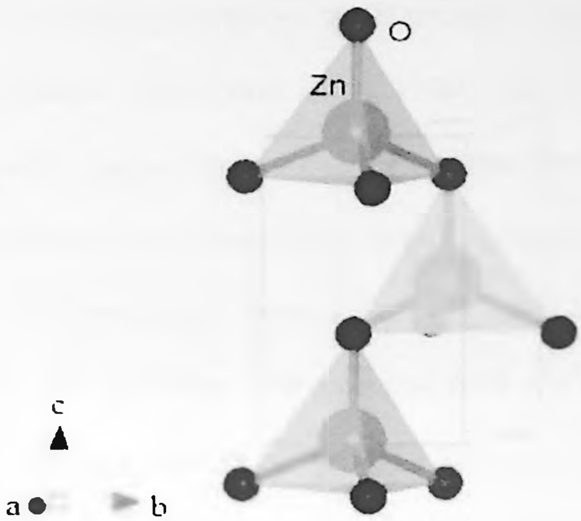

Figure 2.2: Schematic diagram of sp^3 coordination (Hadis and Umit, 2009).

Sun *et al.* reported that there are four (001) surface structures can be displayed in ZnO such as Zn-polar surface with Zn-atoms, Zn polar surface with O-atoms termination, O polar surface with O-atoms termination and O polar surface with Zn-atoms termination as illustrated in Figure 2.3 (Sun *et al.*, 2006). This is because both the Zn and O polar surface can be either Zn or O atom terminated.

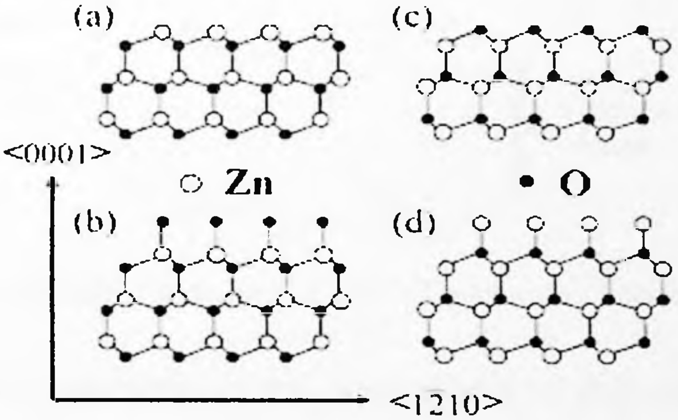

Figure 2.3: ZnO (001) surface structures (a) Zn-polar surface with Zn- atom, (b) Zn polar surface with O atom termination, (c) O polar surface with O atom termination and (d) O polar surface with Zn atom termination (Sun *et al.*, 2006).

The band structure of ZnO determines its electronic state (Thareja and Mohanta, 2010) and potential applications (Hadis and Umit, 2009). ZnO is a wide direct bandgap semiconductor (3.36 eV) with a large binding energy ~60 meV at room temperature. It has the upper most valence and the lowest conduction bands at the same point in the Brillouin zone (Klingshrim, 2007). The bandgap is formed due to the anti-bonding level between Zn 4s orbital and O 2p orbital. The influence of the crystal field and spin orbit coupling cause the valence band of ZnO to split into three bands, i.e. A (Γ7), B (Γ9) and C (Γ7) as illustrated in Figure 2.4 (Thonke and Feneberg, 2011). The conduction band edge (E_{cb}) and valence band edge (E_{vb}) of ZnO is -4.19 eV and -7.39 eV respectively. The properties of ZnO such as density, melting point, thermal conductivity, linear expansion coefficient, static dielectric constant and refraction index are summarized in Table 2.1.

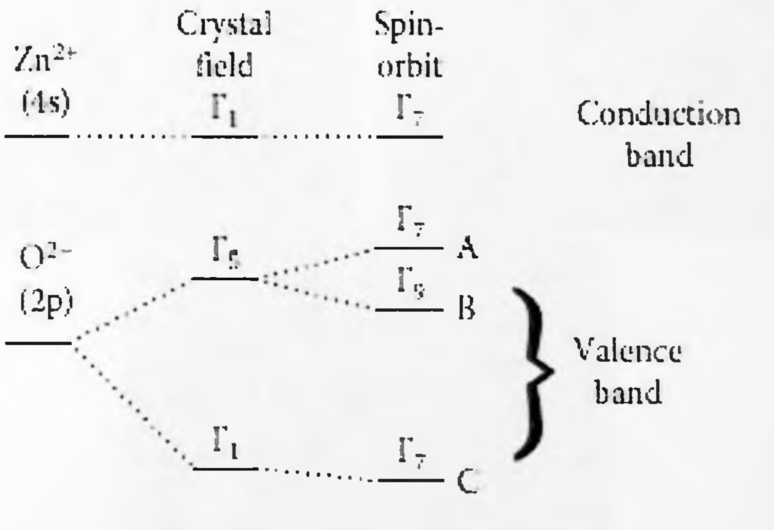

Figure 2.4: Bandgap structure of ZnO (Thonke and Feneberg, 2011).

Pung *et al* has synthesized several morphologies of ZnO using sol gel method as shown in Figure 2.5 by control the concentration of ammonia on the growth of ZnO nanoparticles (Pung *et al.*, 2012). Ammonia provides a basic environment that is necessary for the formation of zinc hydroxyl and plays the role of stabilizer in the aqueous zinc ion

(Xu and Wang, 2011, Zhou *et al.*, 2010). When the ammonia concentration decreased from 2.0 ml to 1.5 ml, ZnO nanoparticles changed from rod-like to cone-like nanoparticles because the ammonia affected the concentration of $Zn(OH)_4^{2-}$ during the forming of ZnO nanoparticles (Pung *et al.*, 2012).

Table 2.1: Properties of ZnO (Pearton *et al.*, 2003).

Property	**Value**
Density (g/cm^3)	5.606
Melting point (°C)	1975
Thermal conductivity (W/(mK))	0.6, 1-1.2
Linear expansion coefficient	a_o: 6.5 x 10^{-6}
	c_o: 3.0 x 10^{-6}
Static dielectric constant	8.656
Refractive index	2.008, 2.029

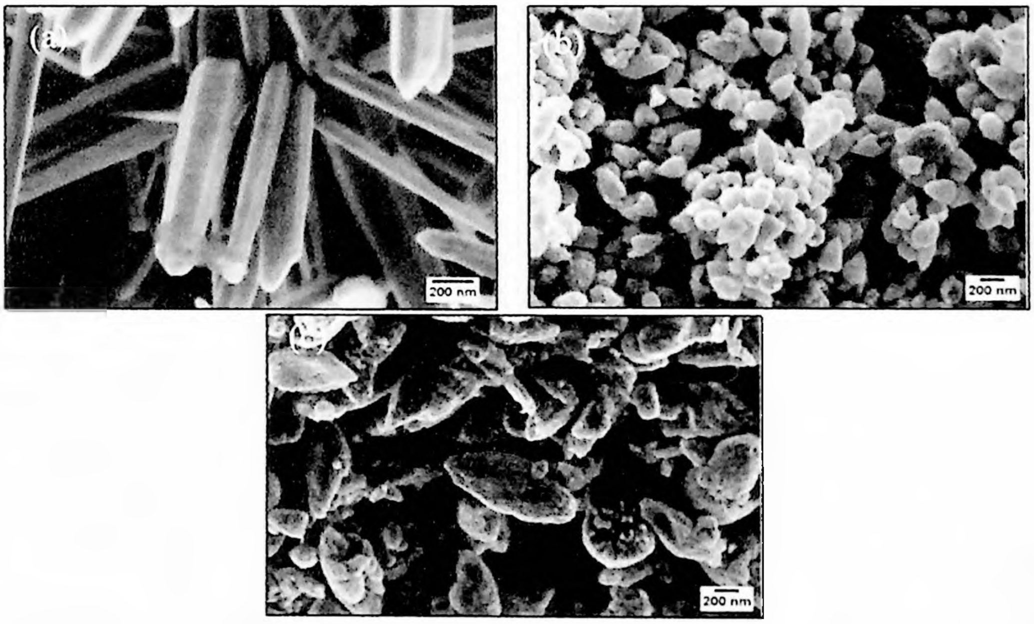

Figure 2.5: The morphologies of ZnO (a) rod-like, (b) cone-like and (c) rice-like nanoparticles (Pung *et al.*, 2012).

2.1.2 Vanadium Oxide (V_2O_5) Nanoparticles

Vanadium oxide (V_2O_5) was first produced via sol-gel method by Ditte in 1885. In this case, ammonium vanadate (NH_4VO_3) was heated in a platinum crucible, then the residue was reacted with hot nitric acid. Finally, it was poured into water. Formation of red sol, i.e. vanadium pentoxide was observed. A few years later, Biltz reported that V_2O_5 sol or gel could be produced using hydrochloric acid. V_2O_5 could be obtained via variety ways such as thermohydrolysis and precipitation (Livage, 1991).

V_2O_5 could to be used as electrode material for lithium rechargeable batteries (Livage *et al.*, 1998, Wang *et al.*, 2005, Wang *et al.*, 2006). This is due to its high energy density, ease of fabrication and relative safe to be used (Olivetti *et al.*, 2006). Besides, it also can be used as optical switching materials such as humidity sensors because of its excellent electrochromic properties (Olivetti *et al.*, 2006).

2.1.2.1 Structural and Chemical Bonding of V_2O_5 Nanoparticles

Vanadium oxide has variety oxidation state from 2+ to 5+ with variety oxygen coordination geometry in forming of VO, V_2O_3, VO_2 and V_2O_5. Thus, V_2O_5 consists variety morphology such as octahedral, pentagonal by pyramids, square pyramids and tetrahedral. This morphology can combine with each other by sharing corners, edge and faces to form structure such as V_8O_{15}, V_7O_{13} and V_6O_{11} (Surnev *et al.*, 2003).

Vanadium oxide with different oxidation state can be formed by adjusting the concentration precursor and pH at room temperature as displayed in Figure 2.6 (Livage, 1991, Takahashi *et al.*, 2005). The structure of V_2O_5 is orthorhombic with oxidation state of $3d^0$ as illustrated in Figure 2.7. It is a zigzag ribbons of square pyramidal of VO_5 units by sharing the edge of VO_5 for building the double chain (Livage, 1991). As shown in Figure 2.6, it consists of three type of V-O bonding with (001) direction as follows:

a) vanadyl ion bonded with 1 oxygen ion along the c-direction (1.58 Å)

b) vanadyl ion bridged with 2 or 3 oxygen ions in the basal plane (1.77 Å to 2.02 Å)

c) vanadyl ion bonded between the layer (weak bond) (2.79 Å)

The electric conductivity and current density of V_2O_5 is 10^{-2} to 10^{-3} S/cm and 0.7 A/g respectively (Wang *et al.*, 2005). When the V_2O_5 is in thin film, the electrical conductivity is ranging from 10^{-6} Ω^{-1} cm^{-1} to approximately 1 Ω^{-1} cm^{-1}(Livage, 1991). The capacitance of amorphous V_2O_5 can reach up from 250 mAh/g to 300 mAh/g which is higher than crystalline V_2O_5 (Wang *et al.*, 2005, Livage, 1991, Livage *et al.*, 1997).

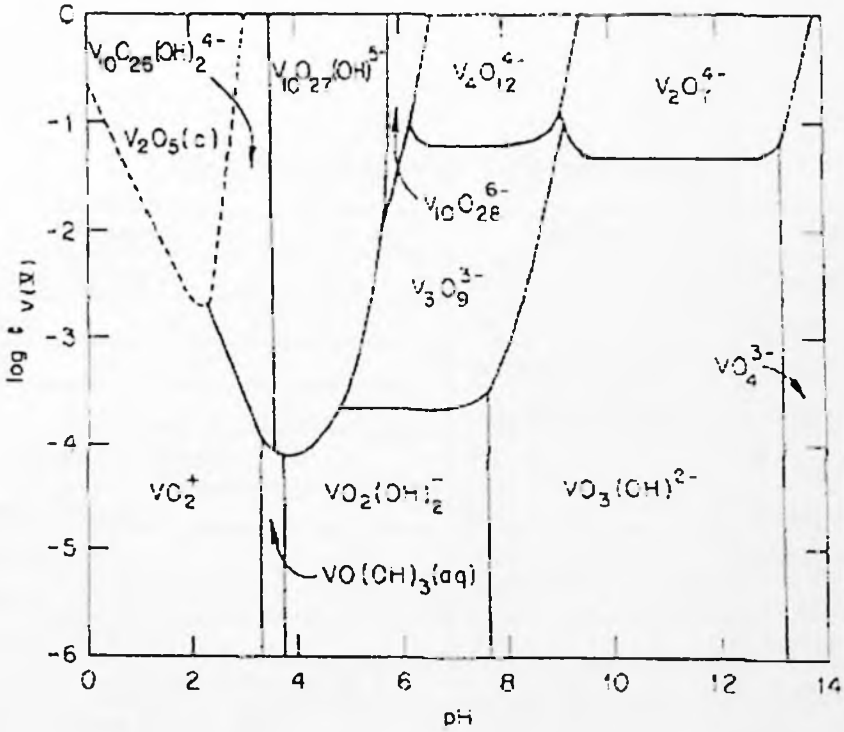

Figure 2.6: Predominant diagram of vanadium oxide (Livage, 1991).

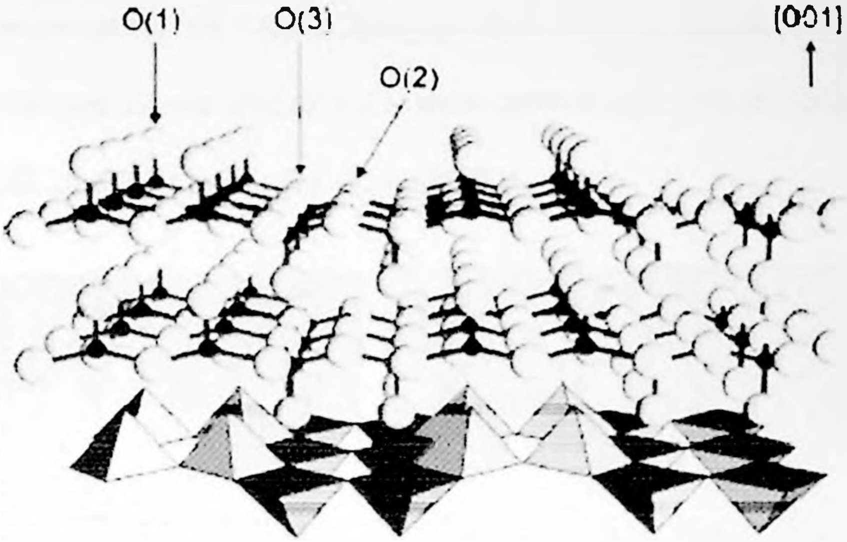

Figure 2.7: Schematic structure of V_2O_5 (Surnev *et al.*, 2003).

The lattice constants of V_2O_5 are 27.0 Å and 3.6 Å for 'a' and 'b' respectively. Proton diffusion coefficient (D) is about 1.6 x 10^{-8} cm^2s^{-1} (Livage, 1991). The V_2O_5 properties have been summarized in Table 2.2. The bandgap of V_2O_5 is 2.80 eV with zig-zag ribbon structure.

Table 2.2: Summary of V_2O_5 properties.

Property	Value	References
Energy bandgap (E_g) (eV)	2.80	(Viswanathan, 2011)
Oxidation state	$3d^0$	(Surnev *et al.*, 2003)
Unit structure	orthorhombic	(Surnev *et al.*, 2003)
Structure	Zig-zag ribbon	(Livage, 1991)
Electrical conductivity (S/cm)	10^{-2} to $1\text{-}0^{-3}$	(Wang *et al.*, 2005)
Current Density (A/g)	0.7	(Wang *et al.*, 2005)
Capacitance (mAh/g)	300	(Wang *et al.*, 2005)
Lattice constant ('a') (Å)	27.0	(Livage, 1991)
Lattice constant ('b') (Å)	3.6	(Livage, 1991)
Proton diffusion coefficient (D) (cm^2s^{-1})	1.6 x 10^{-8}	(Livage, 1991)
Thermoelectric power (TEP) (m^{-3})	1.98 10^{26}	(Bahgat *et al.*, 2005)

Li *et al* reported several morphologies of V_2O_5 nanostructure such as belt-like, olive-like flower-like by controlling the concentration of oxalic acid as shown in Figure

2.8. When the concentration of oxalic acid is 0.05 mol/L, belt-like of V_2O_5 was synthesized. Olive-like and flower-like of V_2O_5 were synthesized with the concentration of oxalic acid 0.08 mol/L and 0.10 mol/L (Li *et al.*, 2007).

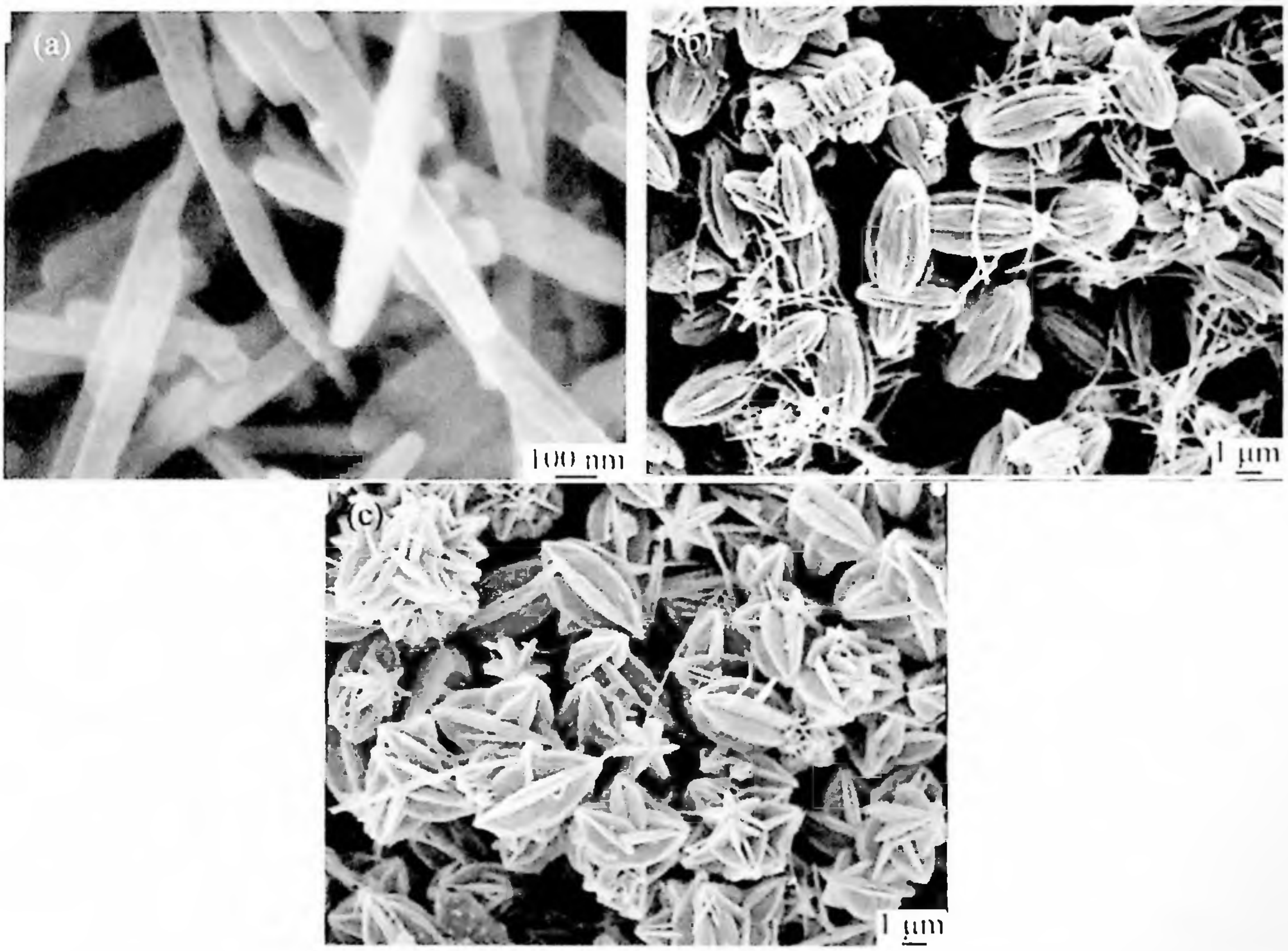

Figure 2.8: The morphologies of V_2O_5 (a) belt-like, (b) olive-like and (c) flower-like (Li *et al.*, 2007).

2.1.3 Manganese (IV) Oxide (MnO_2) Nanoparticles

Manganese (IV) oxide (MnO_2) is a n-type semiconductor (Preisler, 1976). MnO_2 is a nonprecious metal oxide. It can be prepared via manganese salt in pH above 5.5 (Bromfield, 1958, Wadsley, 1950, Xia *et al.*, 2011). Pure MnO_2 was only commercially available in 1941, selling by Shelton (Maris and Jin, 2010).

The application MnO_2 is mainly in capacitor which use to store energy (Zhang *et al.*, 2011). MnO_2 is suitable for charge storage because it has a high specific energy as compared to conventional capacitor (Xia *et al.*, 2011). It has long term stability, which can withstand 1000 cycles with stable capacitances (Toupin *et al.*, 2002). Besides, MnO_2 is environmental friendly compares to transition metal oxide such as ruthenium oxide. MnO_2 also uses as oxidation catalyst since it is effective in oxidation and reusable (Ilyas *et al.*, 2013, Hashemzadeh *et al.*, 2009).

Recently, MnO_2 has been used as photocatalysts under visible light irradiation to degrade organic compound with different type of polymorphs such as β-phase, γ-phase, δ-phase and λ-phase because of its narrow bandgap (Eg = 1.0 to 1.8 eV). With addition of hydrogen peroxide (H_2O_2), Cao *et al* stated that α- and β- MnO_2 can degrade RhB and methylene blue (MB). H_2O_2 is responsible to produce more free radicals to decoloration the dye (Maris and Jin, 2010, Cheng *et al.*, 2010).

2.1.3.1 Structural and Chemical Bonding of MnO_2 Nanoparticles

MnO_2 can present in a few polymorphs such as β-MnO_2 (Tang *et al.*, 2003), δ-MnO_2 (Hashemzadeh *et al.*, 2009), α-MnO_2 (Rossouw *et al.*, 1992) and γ-MnO_2 (Zhou *et al.*, 2007, Preisler, 1976). MnO_2 has a cubic perovskite structure (Cao, 2004), as illustrated in Figure 2.9. The cubic perovskite structure of MnO_2 can be modified when rock salt type block layer is inserted into it. The electronic and magnetic properties of MnO_2 can be approached to infinity with increasing of MnO_2 sheet (Chahara *et al.*, 1993, Goyal *et al.*, 1997). Figure 2.10 demonstrates the structure of MnO with rock salt type block layer. The structure of MnO_2 is in ferromagnetic (nonmetallic) when n=1. The ferromagnetic ground state of MnO_2 causes double-exchange interaction because manganese has many ion states such as Mn^{2+}, Mn^{3+}, Mn^{4+} and Mn^{7+} (Moritomo *et al.*, 1996).

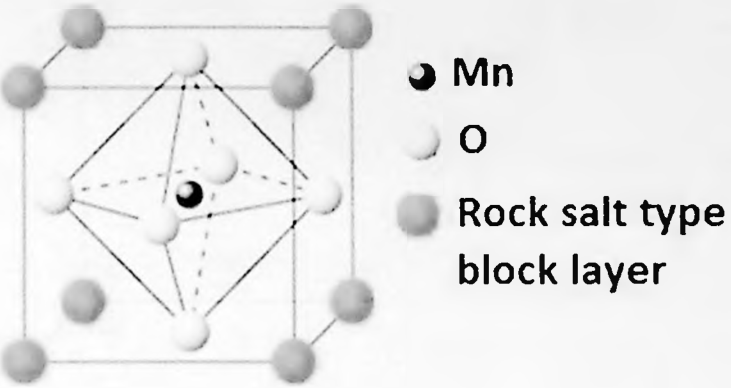

Figure 2.9: MnO_2 structure cubic perovskite structure (Cao, 2004).

Hashemzadeh et al stated that the different polymorphs of MnO_2 such as α-MnO_2 (Hollandite), β-MnO_2 (pyrolusite), δ-MnO_2 (Birnessite) and γ-MnO_2 (Nsutite) can be formed as indicated in Figure 2.11 when the basic units are arranged in different ways {MnO_6} (Owen *et al.*, 2007, Bock *et al.*, 2012, Hashemzadeh *et al.*, 2009). The average oxidation state for edge-shared MnO_6 is 3.7 (Giraldo *et al.*, 2000).

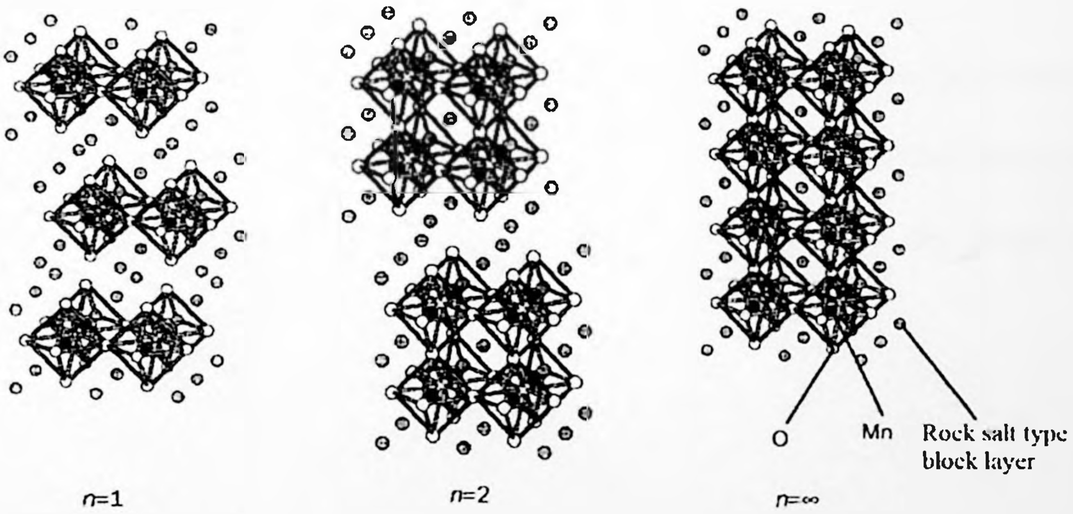

Figure 2.10: Schematic diagram of MnO_2 based layered perovskite when inserted rock salt type block layer (Moritomo *et al.*, 1996).

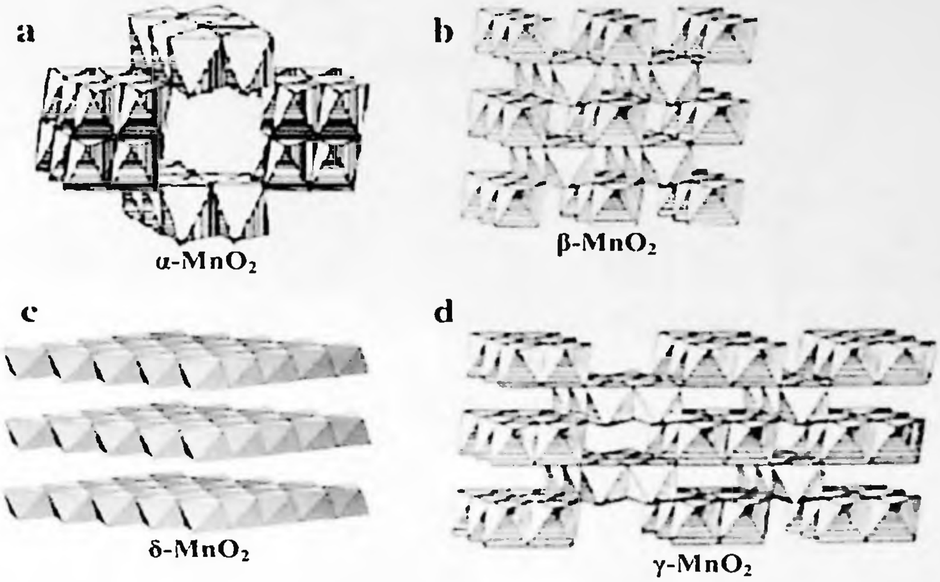

Figure 2.11: Schematic diagram of (a) α-MnO_2 (Hollandite), (b) β-MnO_2 (pyrolusite), (c) δ-MnO_2 (Birnessite) and (d) γ-MnO_2 (Nsutite) (Hashemzadeh *et al.*, 2009).

The specific conductivity of MnO_2 is between 10^{-6} $ohm^{-1}cm^{-1}$ to 10^{3} $ohm^{-1}cm^{-1}$. The conductivity measurement is proportional to density, i.e. between 4.0 $g.cm^{-3}$ to 4.6 $g.cm^{-3}$. The conductivity of MnO_2 increases with the heat treatment temperature. It changes phase from γ-MnO_2 to β-MnO_2 when the temperature increases within 300 to 400 °C (Preisler, 1976).

Several morphologies and phase can be provided when changing the concentration of KCl as reported by Huang *et al.* As shown in Figure 2.12, the rod-like of MnO_2 changed to belt-like when the concentration of KCl increased 4 M. Besides, the phase of MnO_2 changed from β- to α-MnO_2 (Huang *et al.*, 2008).

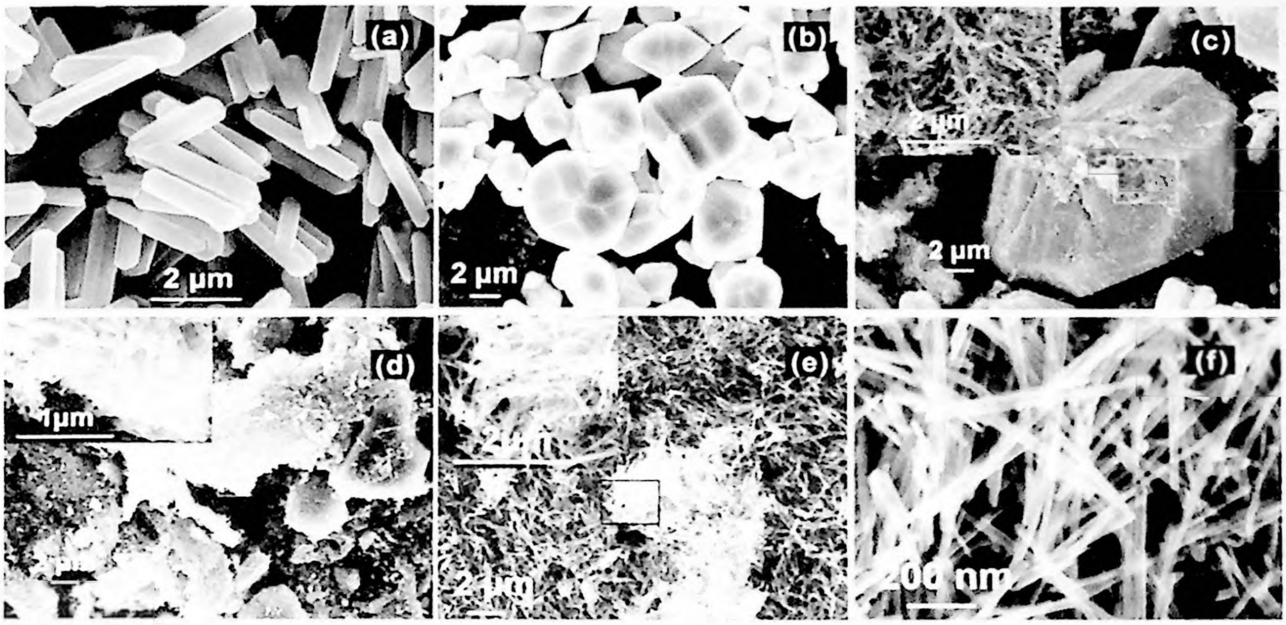

Figure 2.12: SEM images of (a)–(b) β-, (c)–(d) α/β- and (e)–(f) α-MnO_2 obtained in the presence of 0, 0.1, 0.23, 0.25, 0.27 and 4 M KCl, respectively (Huang *et al.*, 2008).

2.2 Synthesis of Nanomaterials using Solution Route

Nanomaterials could be synthesized using solution route such as sol gel synthesis, hydrothermal process and electro-deposition technique. Generally, these techniques offer advantages such as low setup cost, low synthesis temperature and capable of mass production. However, the nanomaterials produce in solution route relatively have a poorer crystallinity and contamination as compared to vapor route synthesis.

2.2.1 Sol Gel Approach

Sol gel process has been used by researchers to synthesis variety materials such as ZnO, TiO_2, CeO_2, Cr_2O_3 and CdS since late 1880s (Gupta and Kumar, 2010). In this process, a liquid "sol" is transformed into a solid "gel" based on the hydrolysis and condensation of reactions of precursors. Sols are colloidal suspension of solid particles in a liquid. The interactions of these sol particles are dominated by short range forces such as

Van der walls and electrostatic forces. This is attributed to a very small size of dispersed phase in the range of 1 nm^{-1}. Gels are the integrated networks (semi solid and liquid) consisting of continuous solid and liquid phases of colloidal formed by condensation reaction.

Precursors use in sol gel process are inorganic metal salts or metal organic compounds such as alkoxide {$M(OR)_n$} (M: network former and R: alkyl group) (Cao, 2004). These precursors involve in a polymerization reaction to form a colloidal suspension. During this polymerization, hydroxyl ions are attached to the metal atoms. Thus, this reaction is also known as hydrolysis process as indicated in Equation (2.1).

$$M(OR)_x + H_2O \leftrightarrow HO - M(OR)_{x-1} + ROH \qquad (2.1)$$

where ROH is alcohol.

As shown in Equation (2.2), the OR groups can be replaced by OH ions to complete the hydrolysis process, depending on the amount of precursor and water present in the solution.

$$M(OR)_x + xH_2O \leftrightarrow M(OH)_x + xROH \qquad (2.2)$$

Either precipitation or solvent evaporation methods can be used to form nanoparticles via sol gel approach as illustrated in Figure 2.13 (Ashby *et al.*, 2009). In precipitation method, the particles are extracted or spin-coated onto the substrate from the sol colloidal suspension. These particles will later solidify. In solvent evaporation process, extended network is formed by attractive forces to connect the particles to form superpolymer or 3-D network during gelling process. Condensation reaction during gelling process is represented in Equations (2.3) and (2.4).

$$(OR)_{x-1}M - OH + HO - M(OR)_{x-1} \leftrightarrow (OR)_{x-1}M - O - M(OR)_{x-1} + H_2O \quad (2.3)$$

$$(OR)_{x-1}M - OR + HO - M(OR)_{x-1} \leftrightarrow (OR)_{x-1}M - O - M(OR)_{x-1} + ROH \quad (2.4)$$

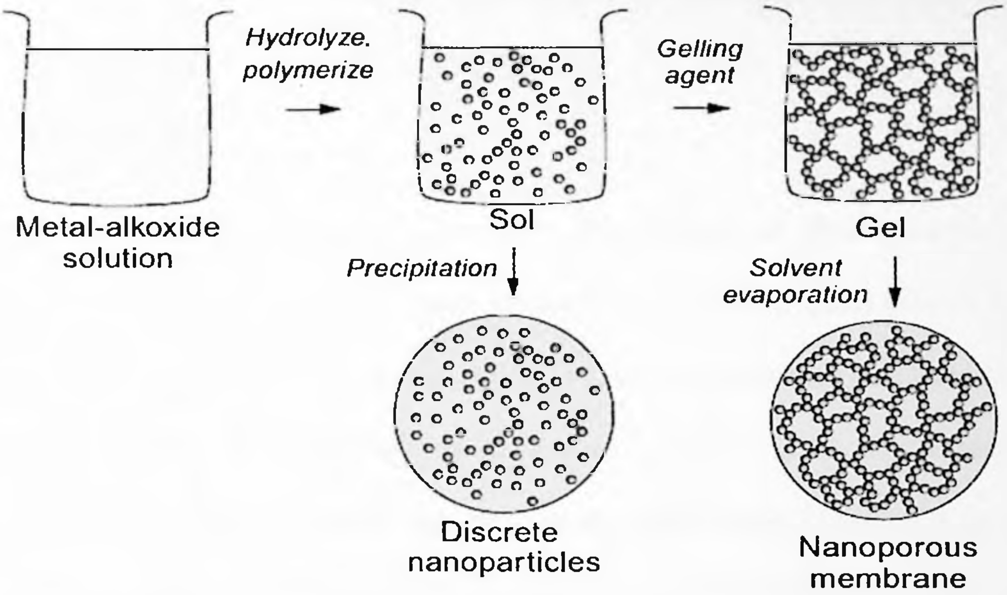

Figure 2.13: Illustration of sol gel process (Ashby *et al.*, 2009).

Fu *et al.* produced ZnO rice-like nanostructures via sol gel method using zinc nitrate hexahydrate ($Zn(NO_3).6H_2O$) and hexamethylenetetramine (HMTA, $(CH_2)_6N_4$) as precursor at at 90 °C for 3 h (Fu *et al.*, 2011). The zinc nitrate hexahydrate dissociates into Zn^{2+} ions. HMTA is a non-ionic cyclic tertiary amine which acts as bidentate Lewis base, producing NH_3. The NH_3 is subsequently hydrolyzed to form NH^{4+} ions and OH^- ions as shown in Equations (2.5) and (2.6). HMTA plays two important roles to produce ZnO nanostructures: (i) to produce a basic environment that is necessary for the formation of

$Zn(OH)_2$ and (ii) to stabilize Zn^{2+} ions in the aqueous solution as shown in Equation (2.7) and (2.8). Finally, ZnO nanoparticles are formed.

$$(CH_2)_6N_4 + 6H_2O \overset{\Delta T}{\leftrightarrow} 6CH_2O + 4NH_3 \tag{2.5}$$

$$NH_3 + H_2O \leftrightarrow NH_4^+ + OH^- \tag{2.6}$$

$$Zn^{2+} + 2OH^- \leftrightarrow Zn(OH)_2 \tag{2.7}$$

$$Zn(OH)_2 \overset{\Delta T}{\rightarrow} ZnO + H_2O \tag{2.8}$$

Generally, there are 2 stages in growing 1-dimensional of ZnO nanomaterials via sol-gel process on the substrate such as paper (Baruah *et al.*, 2010), glass (Hu *et al.*, 2010), Indium tin oxide (ITO) (Hung and Whang, 2003), i.e.: (i) deposition of ZnO seed layer and (ii) subsequent growth of nanomaterials as illustrated in Figure 2.14. For instance, ZnO seed nanoparticles could be deposited sing zinc acetate dehydrate ($Zn(CHOO)_2.2H_2O$) as precursor and alcoholic (ethanol) as solvent (Baruah *et al.*, 2010, Hung and Whang, 2003). In another example, sodium hydroxide (NaOH) which was an alkaline solution was added into the solution for the formation of ZnO seed nanoparticles (Laudise and Ballman, 1960). The substrate was subsequently immersed into the solution and was heated to improve the adhesion of the ZnO seed layer on the substrate (Han *et al.*, 2012).

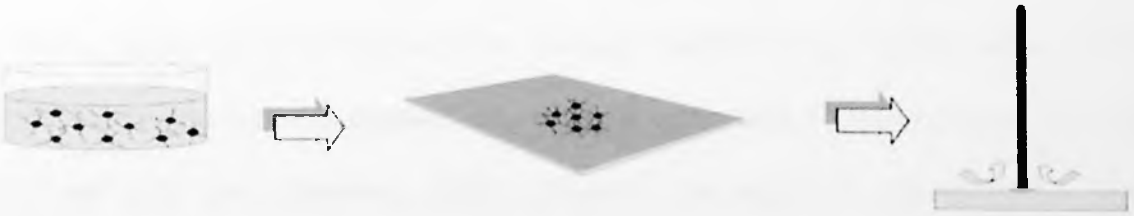

Figure 2.14: The schematic of growing ZnO nanostructure on the substrate (Hung and Whang, 2003).

Synthesis of V_2O_5 via sol gel method was normally conducted using alkoxyvanadate as precursors such as vanadium oxytrichloride and vanadium triisopropoxide (Agrawal *et al.*, 1993, Niederberger *et al.*, 2000, Zilberberg *et al.*, 2011). Niederberger *et al* reported that V_2O_5 could synthesized by mixing of vanadium oxytrichloride ($VOCl_3$) with primary amine ($C_nH_{2n+1}NH_2$) where "n" is between integer 11 to 16. The solution was stirred until it was formed brown viscous solution. Then, acetate buffer was added into it under vigorous stirring. Precipitate occurred and it was aged for 7 days. Finally, V_2O_5 nanotubes were formed (Niederberger *et al.*, 2000). Krumeich *et al* stated that vanadium (V) trisopropoxide and primary amine ($C_nH_{2n+1}NH_2$) where "n" is between integer 4 to 22 was used to synthesize V_2O_5 nanoparticles. The solution was stirred for 1 h and resulted yellow solution. The yellow solution was hydrolyzed and then aged for 12 to 96 h. The result was an orange hydrolyzed vanadium oxide (Krumeich *et al.*, 1999).

In addition, vanadium sulfate ($VOSO_4.nH_2O$) could be used as starting material with sulfuric acid as solvent to synthesis V_2O_5 nanotubes on the substrate. Vanadium ion (VO^{2+}) is produced from $VOSO_4.nH_2O$. VO^{2+} would react with water to form V_2O_5 as dedicated in equation (2.9) (Wang *et al.*, 2005, Lee *et al.*, 2005).

$$2VO^{2+} + 3H_2O \rightarrow V_2O_5 + 6H^+ + 2e^- \tag{2.9}$$

MnO_2 could also synthesized be sol-gel method. The molar ratio of 1:2 of manganese acetate manganese acetate (MnAc) and citric acid ($C_6H_7O_8$) were dissolved in distilled water and then ammonia (NH_3) solution was added to the solution until the solution reached pH 6. Next, it was stirred and heated at 80 °C until a wet gel was formed.